Atmos. Chem. Phys. Discuss., 12, 13363–13403, 2012
www.atmos-chem-phys-discuss.net/12/13363/2012/
doi:10.5194/acpd-12-13363-2012

Atmospheric Chemistry and Physics Discussions

Profiling of fine and coarse particle mass: case studies of Saharan dust and Eyjafjallajökull/Grimsvötn volcanic plumes

A. Ansmann[1], **P. Seifert**[1], **M. Tesche**[2], **and U. Wandinger**[1]

[1]Leibniz Institute for Tropospheric Research, Leipzig, Germany
[2]Department of Applied Environmental Science, Stockholm University, Stockholm, Sweden

Received: 7 May 2012 – Accepted: 16 May 2012 – Published: 30 May 2012

Correspondence to: A. Ansmann (albert@tropos.de)

Published by Copernicus Publications on behalf of the European Geosciences Union.

Abstract

The lidar-photometer method introduced to separate volcanic coarse-mode and fine-mode particle properties is extended to cover Saharan dust events as well. A review of recently published mass-specific extinction coefficients for Saharan dust and volcanic dust is presented. These mass-specific extinction coefficients are required in the retrieval of particle mass concentration profiles. Case studies of four different scenarios corroborate the applicability of the profiling technique: (a) Saharan dust outbreak to Central Europe, (b) Saharan dust plume mixed with biomass-burning smoke over Cape Verde, and volcanic aerosol layers originating from (c) the Eyjafjallajökull eruptions in 2010 and (d) the Grimsvötn eruptions in 2011. Strong differences in the vertical aerosol layering, aerosol mixing, and optical properties are observed for the different volcanic events.

1 Introduction

The eruptions of the Eyjafjallajökull volcano in April–May 2010 triggered the development of a variety of new lidar-based methods to identify ash and dust particles[1] in volcanic aerosol plumes containing fine and coarse particles. These new lidar profiling techniques further allow us to quantify the optical properties of the volcanic ash and dust particles (coarse-mode) and to estimate their mass concentration (Ansmann et al., 2011a; Gasteiger et al., 2011; Marenco and Hogan, 2011; Miffre et al., 2011; Chaikovsky et al., 2012; Wagner et al., 2012).

Two lidar methods are of fundamental importance in this context. The polarization lidar technique permits the discrimination of non-spherical, light-depolarizing, coarse-mode particles such as volcanic dust and desert dust and spherical,

[1] Ash and dust particles have diameters $> 60\,\mu m$ and $< 60\,\mu m$, respectively. By the same diameter of 60 µm, desert sand and dust particles (silt-sized and background dust) are separated.

ACPD
12, 13363–13403, 2012

non-light-depolarizing fine-mode particles such as anthropogenic haze and sulfate particles originating from the volcanic SO_2 emissions (Murayama et al., 1999; Sugimoto et al., 2003; Shimizu et al., 2004; Sugimoto and Lee, 2006; Sassen, 2005; Sassen et al., 2007; Nishizawa et al., 2007; Liu et al., 2008; Freudenthaler et al., 2009; Groß et al., 2011a, 2012; Miffre et al., 2012). Furthermore, the profiles of the backscatter coefficient of coarse-mode and fine-mode particles can be separated (Tesche et al., 2009b, 2011b).

The second important lidar method is the aerosol Raman lidar technique (Ansmann and Müller, 2005) which allows us to independently measure particle backscatter and extinction coefficients and thus provides important (benchmark-like) data on the relationship between the backscatter and the extinction coefficient of pure desert dust, pure volcanic dust, and mixtures of coarse-mode and fine-mode particles (Mattis et al., 2002, 2010; Pappalardo et al., 2004; Müller et al., 2007; Wang et al., 2008; Tesche et al., 2009a, 2011a; Wiegner et al., 2011a,b; Groß et al., 2011b, 2012; Mona et al., 2012; Papayannis et al., 2012; Sicard et al., 2012). The importance of Raman lidar observations arise from the fact that profiles of the particle backscatter coefficient are widely measured with standard (Mie) backscatter lidar and advanced ceilometers, but the particle extinction coefficient is required to estimate the mass concentration (via mass-specific extinction coefficients) (Barnaba and Gobbi, 2004). Thus, extinction-to-backscatter ratios (lidar ratios) are needed to convert backscatter profiles into extinction profiles and these into mass concentration profiles.

A few Raman lidars (at supersites) of a potential aerosol monitoring network consisting mostly of small standard backscatter lidars and ceilometers are sufficient to provide the necessary lidar-ratio information. The potential to measure polarized and Raman-backscattered light at several wavelengths simultaneously further increases the ability of lidar to unambiguously separate fine-mode and coarse-mode particles and to quantify the aerosol properties in detail (Tesche et al., 2009b, 2011b; Veselovskii et al., 2010, 2012; Gasteiger et al., 2011; Wiegner et al., 2011a; Groß et al., 2011a; Chaikovsky et al., 2012).

ACPD
12, 13363–13403, 2012

A powerful aerosol remote sensing station is equipped with lidar and Sun photometer (Müller et al., 2003). Photometers provide spectrally resolved column-integrated particle extinction values (aerosol optical thickness, AOT) as well as AOT-related scattering-phase-function information at several wavelengths. They permit the retrieval of fine-mode- and coarse-mode-related AOTs (O'Neill et al., 2003; Dubovik et al., 2006) and of microphysical particle properties such as volume and surface-area concentrations for the coarse-mode and fine-mode fractions (Dubovik and King, 2000; Dubovik et al., 2006). Toledano et al. (2011, 2012) demonstrate the usefulness of Sun photometry in cases of complex aerosol scattering conditions. It has been shown that the combination of polarization lidar and Sun photometry is a robust and comparably simple technique to separate coarse-mode and fine-mode particle fractions with vertical resolution and to retrieve profiles of coarse and fine particle mass concentrations (Ansmann et al., 2011b).

Here we present a more general approach to our lidar-photometer method which was successfully applied to European Aerosol Lidar Network (EARLINET) observations of the Eyjafjallajökull volcanic aerosol plumes in Central and Southwestern Europe (Ansmann et al., 2011b; Sicard et al., 2012). We now include applications to Saharan dust. In the course of the discussion, an extended review of recent observations of mass-specific extinction coefficients for Saharan and volcanic dust is presented. Such specific extinction coefficients are required to convert measured particle optical properties into microphysical information. After the introduction of the methodology in Sect. 2, applications of the technique are discussed in Sect. 3. These case studies include unique observations of (a) a lofted, almost pure Saharan dust plume as typically observed over Central Europe after Saharan dust outbreaks (Ansmann et al., 2003; Papayannis et al., 2008; Wiegner et al., 2011b), (b) mixtures of desert dust with biomass-burning aerosol as observed at Cape Verde during the Saharan Mineral Dust Experiment 2 (SAMUM-2) (Ansmann et al., 2011a; Tesche et al., 2011a,b; Groß et al., 2011a,b), and (c) and (d) volcanic aerosol plumes (mixtures of volcanic dust and sulfate particles) after the Eyjafjallajökull volcanic eruption in April 2010 (Ansmann et al., 2011b) and

ACPD
12, 13363–13403, 2012

after the eruptions of the Grimsvötn volcano on Iceland in May 2011 (Kerminen et al., 2011; Tesche et al., 2012).

2 Method

The instruments, retrieval methods, and uncertainties are discussed in detail by Ansmann et al. (2011b). In this section, we briefly summarize the data processing scheme and extend the methodology towards pure and mixed desert dust aerosols. An overview of the different steps of the retrieval procedure is given in Table 1.

The basic idea of the method is to use the depolarization ratio measured with lidar for the identification of layers with non-spherical particles and to quantify their contribution to the determined profile of the volume backscatter coefficient of particles. This part of the data analysis is covered by steps 1–4 in Table 1.

The assumption that the fraction of light-depolarizing, non-spherical particles is identical with the coarse-particle fraction is of fundamental importance in the retrieval. According to this assumption, the coarse-mode AOT derived from the photometer observations is caused by light extinction by non-spherical particles and the derived coarse-mode particle volume concentration describes the volume concentration of non-spherical particles. Consequently, we assume that the lidar-derived fraction of non-depolarizing, spherical particles is identical with the fine-mode particle fraction and is thus responsible for the fine-mode AOT. This approach holds for continental aerosols, e.g., for mixtures of desert dust and biomass-burning smoke (Tesche et al., 2009b, 2011b) and mixtures of volcanic dust and urban haze (Ansmann et al., 2011b). The assumption is not valid for aerosols containing non-depolarizing, coarse particles, e.g., marine aerosol. It is worth mentioning that coarse marine particles (sea salt particles) in the humid marine boundary layer are always covered by a spherical water shell so that their depolarization ratio is zero. This is corroborated by field observations (Groß et al., 2011b) and laboratory studies (Sakai et al., 2010).

ACPD
12, 13363–13403, 2012

In our data analysis, we assume an externally mixed aerosol which contains only one type of coarse-mode particles. In order to retrieve the mass concentration of desert dust we must be sure that the influence of marine and volcanic particles on the measured optical properties is negligible. Vice versa, in the estimation of volcanic particle mass concentrations we have to assume that interference by desert dust and marine particles can be ignored. This assumption was, for example, not fulfilled in the case of Eyjafjallajökull volcanic measurements over Southeastern Europe in April and May 2010 (Papayannis et al., 2012). Volcanic dust and desert dust occurred simultaneously and contributed to the observed coarse-mode fraction.

Steps 1–3 of our retrieval (see Table 1) are straightforward and well-established lidar methods. In step 4, the backscatter contributions of the non or weakly light-depolarizing particles (e.g., urban haze and biomass-burning smoke) and the strongly light-depolarizing particles (e.g., volcanic or desert dust) are separated. Here, we have to assume characteristic particle depolarization ratios. For desert dust, we use a value of 0.31 ± 0.03 (Freudenthaler et al., 2009; Groß et al., 2011b), for volcanic dust 0.34 ± 0.03 (Ansmann et al., 2010; Wiegner et al., 2011a; Groß et al., 2012), and for fine-mode and marine particles 0.02 ± 0.02 (Groß et al., 2011b).

In step 5 of the retrieval after Table 1, we estimate the profiles of the volume extinction coefficients σ_f and σ_c for fine and coarse mode by multiplying the fine and coarse particle backscatter coefficients β_f and β_c with respective fine and coarse particle lidar ratios. Raman lidar observations indicate lidar ratios from 45 to 65 sr for desert dust and volcanic dust. The values accumulate between 50 and 60 sr (Tesche et al., 2009a; Ansmann et al., 2010; Groß et al., 2011b, 2012; Wiegner et al., 2011b). The range of values for the fine-mode particle lidar ratio is much larger. Urban haze particles show values from 30 to 80 sr (Müller et al., 2007). Lidar ratios of absorbing biomass-burning smoke may often exceed 100 sr (Ansmann et al., 2000; Franke et al., 2003; Tesche et al., 2011b). Consequently, we must use the actual lidar and photometer observations to estimate the most appropriate fine-mode lidar ratio. This fine-mode lidar ratio is obtained from the ratio of the fine-mode AOT (from photometer observations) and the

ACPD
12, 13363–13403, 2012

vertically integrated backscatter coefficient for non-depolarizing particles (from the lidar observations.) This point is further discussed in Sect. 3.

In step 7 of the retrieval (step 6 is explained afterwards), the mass concentrations m_f and m_c of fine-mode and coarse-mode particles, respectively, are estimated by using the lidar-derived particle extinction coefficients σ_f and σ_c:

$$m_f = \frac{\sigma_f}{k_{ext,f}}, \quad (1)$$

$$m_c = \frac{\sigma_c}{k_{ext,c}}. \quad (2)$$

$k_{ext,f} = \sigma_{ext,f}/(\rho_f V_f)$ and $k_{ext,c} = \sigma_{ext,c}/(\rho_c V_c)$ are the mass-specific extinction coefficients for fine mode and coarse mode, respectively. $\sigma_{ext,f}$ and $\sigma_{ext,c}$ denote the volume extinction coefficients that are caused by the respective particle mass densities $\rho_f V_f$ and $\rho_c V_c$. ρ and V are particle density and particle volume concentration, respectively.

We use ρ_c of 2.6 g cm^{-3} for desert dust (Hess et al., 1998; Gasteiger et al., 2011) and volcanic dust particles (Ansmann et al., 2011b). For fine-mode particles, we assume ρ_f of 1.5–1.6 g cm^{-3} (Cozic et al., 2008; Bukowiecki et al., 2011) for Central European haze and for the sulfate aerosol which formed from the volcanic SO_2 emissions. These values of ρ_f consider a variable liquid water content of the mostly sulfate-containing particles (ammonium sulfate) (Hess et al., 1998; Tang and Munkelwitz, 1994). The water content increases with ambient relative humidity. In the analysis of a mixed aerosol plume containing desert dust and biomass-burning smoke in Sect. 3, we use ρ_f of 1.35 g cm^{-3} for the biomass-burning particles (Reid et al., 2005).

The ratios $\sigma_{ext,f}/V_f$ and $\sigma_{ext,c}/V_c$ can vary significantly as a function of particle size distribution (Barnaba and Gobbi, 2004). Thus, actual estimates of these ratios are required in the data analysis. As proxies for $\sigma_{ext,c}/V_c$ and $\sigma_{ext,f}/V_f$ we use the AERONET observations of the ratio of AOT τ_c to the column-integrated volume concentration v_c for the coarse mode and the respective observed ratio τ_f/v_f for the fine mode. Equations (1)

ACPD
12, 13363–13403, 2012

and (2) can then be written as (Ansmann et al., 2011b)

$$m_f = \rho_f(\overline{v_f/\tau_f})\sigma_f, \quad (3)$$

$$m_c = \rho_c(\overline{v_c/\tau_c})\sigma_c. \quad (4)$$

$\overline{v/\tau}$ denotes the temporal mean value of individual values of v/τ observed within a given time period. Time series of observed values of v_f/τ_f and v_c/τ_c for the desert dust and volcanic dust events discussed in Sect. 3 are presented in Fig. 1.

The comparably weak variability in the Saharan dust v/τ ratios in Fig. 1 (cases a and b) found at sites close to the source as well as at remote locations and the likewise strong changes in the volcanic v/τ ratio motivated us to review the recent literature concerning observed and modelled mass-specific extinction coefficients for desert dust and volcanic dust and to re-analyze own AERONET Sun photometer observations performed during strong Saharan dust outbreaks at Leipzig in October 2001 (Ansmann et al., 2003; Müller et al., 2003) and May 2008 (Wiegner et al., 2011b) and during the SAMUM-1 (close to the desert dust source region) and SAMUM-2 campaigns (long-range transport regime). Table 2 provides an overview of this effort. Only a few, carefully selected Saharan dust observations are considered to assure a negligible contamination with anthropogenic fine-mode particles. However, airborne in-situ observations may suffer from high uncertainties in the retrieval of the entire particle size spectrum and the subsequent retrieval of the coarse-mode particle volume concentration. As a consequence, we used the accurate SAMUM-1 $PM_{2.5}$ (particles with diameters $< 2.5\,\mu m$) observations of Weinzierl et al. (2009) in Table 2 instead of the results for the entire size distribution and multiplied the respective $PM_{2.5}$ volume concentration by a factor of 3.1 to estimate the total volume concentration (as considered in Table 2). This factor of 3.1 was derived from ground-based SAMUM-1 and SAMUM-2 observations (Kandler et al., 2009, 2011).

Saharan dust k_{ext} values accumulate between 0.45 and 0.65 $m^2\,g^{-1}$ disregarding the distance of the observation from the source, whereas the values for volcanic dust are

ACPD
12, 13363–13403, 2012

more equally distributed from 0.4 to 1.0 (Johnson et al., 2012; Gasteiger et al., 2011). All values, except the ones from the study of Hervo et al. (2012), are based on the assumption of a coarse-particle mass density of 2.6 g m^{-3}. Hervo et al. (2012) provide mass-specific extinction coefficients for volcanic dust derived from measurements without assumptions on particle mass density. However, they derived the specific extinction coefficients for the wavelength of 355 nm. In Table 2, we assume that these values still hold for 500–550 nm (i.e., we assume no wavelength-dependence of the extinction coefficient and AOT for coarse particles).

Volcanic particle size distributions seem to vary strongly depending on the distance to the source and eruption type (explosive, less explosive, ice-capped explosion or not). The significant difference between coarse-mode v/τ values after the Eyjafjallajökull and Grimsvötn volcanic eruptions in Fig. 1 corroborate this hypothesis. The larger the particles the larger the ratio v/τ, and the lower the mass-specific extinction coefficient (provided the mass density of the volcanic dust particles is similar for both volcanic events).

Even for fine particles (urban haze, biomass-burning smoke, fresh and aged sulfate aerosol originating from volcanic SO_2 emissions) the v/τ values can vary within a factor of two (see Table 2 and Fig. 1, Helgoland and Hamburg versus Leipzig values). The model simulations by Barnaba and Gobbi (2004) in Table 2 with $k_{ext,f}$ values from 3.0–4.0 m^2 g^{-1} consider the full range of realistic size distributions of aged fine-mode European haze.

The spread of the k_{ext} values in Table 2 for a given aerosol type may provide an impression about the range of uncertainty in the particle mass retrieval after Eqs. (4) and (3) when using literature values in the data analysis. Our strategy is therefore to always check the actual values of v_f/τ_f and v_c/τ_c from Sun photometer observations performed side by side with the lidar observations.

A detailed discussion of uncertainties in the retrieval of mass concentrations of desert dust and volcanic dust after steps 1–7 in Table 1 can be found in Tesche et al. (2009b) and Ansmann et al. (2011b). Uncertainties arise from the determination of the

ACPD
12, 13363–13403, 2012

backscatter coefficients by using measured volume depolarization ratios and assuming depolarization ratios representative for fine and coarse mode, from uncertainties in the lidar-ratio estimates applied to obtain the extinction coefficients, from the estimation of particle mass densities, and from uncertainties in the photometer-derived v/τ ratios. In the worst case with relative errors of 20 % in the retrieval of the backscatter coefficients, 20 % in the successive conversion to extinction coefficients, 25 % in the mass density estimates, and 50 % in the used v/τ ratio, the overall uncertainty is 60–70 %. In a realistic scenario with supporting Raman lidar observation of the particle lidar ratio (10 % uncertainty), actual AERONET observations of v/τ (10 % uncertainty), actual column lidar ratios from combined lidar-photometer measurements (10 % uncertainty), and realistic uncertainties of 10 % in the particle density estimates, the relative errors of the coarse and fine particle mass concentrations is of the order of 20–25 %.

3 Measurement examples

We present four exemplary measurement cases. Two cases deal with Saharan dust. The third and fourth examples show volcanic aerosol measurements and, for the first time, comparisons of lidar-photometer observations performed after the Eyjafjallajökull volcanic eruptions in April 2010 with observations at Leipzig after the Grimsvötn volcanic eruptions in May 2011. All heights are given above ground level.

3.1 Saharan dust above urban haze

The retrieved particle properties of a Saharan dust outbreak towards Central Europe are shown in Fig. 2. This outbreak is also discussed in detail by Wiegner et al. (2011b) based on Munich Raman lidar observations about 400 km south of Leipzig. A clear separation of the boundary layer (reaching to 500 m height) and the lofted Saharan dust layer (extending from 500 to 6500 m height) was observed over Leipzig on 29 May 2008.

ACPD
12, 13363–13403, 2012

The Raman lidar method was applied to determine the height profile of the total particle backscatter coefficient in Fig. 2a (retrieval step 2 after Table 1). The Raman lidar method could be used in all four example cases, even during daytime measurements of the volcanic aerosol discussed below. The technique provides most accurate solutions for the backscatter coefficient down to very low heights (if the lidar is well adjusted as is the case here).

By assuming depolarization ratios of 31 % and 2 % for pure Saharan dust and anthropogenic haze, respectively, we separated the particle backscatter coefficients for coarse mode and fine mode (retrieval step 4 after Table 1). It can be seen in Fig. 2c that traces of anthropogenic particles or other spherical fine-mode particles are present in the lower part of the dust plume up to 3 km height, probably caused by upward mixing of polluted air during the transport over Northern Africa, the Mediterranean, and Southern Europe.

In the conversion of the backscatter profiles into extinction profiles (retrieval step 5) we assumed a volcanic-dust lidar ratio of 55 sr and a fine-mode lidar ratio of 65 sr. The profiles of the particle extinction coefficients for fine and coarse mode are shown in Fig. 2d.

The particle mass concentrations for desert dust and the fine-mode particle fraction are computed by using the information shown in Fig. 1 (case b, retrieval steps 6). With $\rho_c = 2.6\,\mathrm{g\,cm^{-3}}$, $\rho_f = 1.6\,\mathrm{g\,cm^{-3}}$, and mean values of $v_c/\tau_c = 0.74 \times 10^{-6}$ m and $v_f/\tau_f = 0.29 \times 10^{-6}$ m we obtain a mass-specific extinction coefficient of $k_{ext,c} = 0.52\,\mathrm{m^2\,g^{-1}}$ and $k_{ext,f} = 2.19\,\mathrm{m^2\,g^{-1}}$ for the coarse and fine mode, respectively. By using these numbers in the conversion of the extinction coefficients into mass concentrations after Eqs. (4) and (3) we end up with the mass profiles in Fig. 2e (retrieval step 7).

As can be seen in Fig. 2e desert dust mass concentrations of up to 300–500 $\mu\mathrm{g\,m^{-3}}$ were observed in the late evening of 29 May 2008. The fine-mode mass concentration reached values of 100 $\mu\mathrm{g\,m^{-3}}$ close to the surface, decreased with height, and was found to be almost zero at heights above 1 km. On days with Saharan dust we frequently observe an almost complete suppression of the boundary-layer evolution. The

ACPD
12, 13363–13403, 2012

anthropogenic haze layer, in which the pollution accumulates over days and remains trapped, is then rather shallow with depths < 1 km.

In order to prove the overall consistency of the lidar-photometer observations and to check the validity of the assumption that the non-light-depolarizing particle fraction is identical with the fine-mode fraction and that the light-depolarizing particle fraction represents the coarse particle fraction, we compute the column-integrated backscatter coefficient (CB) at 532 nm from the fine-mode and coarse-mode backscatter profiles (obtained in retrieval step 4, Table 1) and form the AOT/CB ratios by using the corresponding 532 nm AOTs for fine-mode and coarse mode, obtained from the photometer observation. The 532 nm AOTs (total, fine, coarse in Table 3) are obtained from the measured 500 nm AOTs by means of the retrieved Ångström exponents (O'Neill et al., 2003). Table 3 shows the 532 nm values for CB, AOT, AOT/CB, and the Ångström exponent. The coarse-mode Ångström exponent is set to zero in the photometer data analysis (O'Neill et al., 2003). The column lidar ratio AOT/CB is by definition the backscatter-coefficient-weighted vertical mean extinction-to-backcatter ratio (Ansmann, 2006). This means that layers with strong backscattering control the column lidar ratio.

As can be seen in Table 3, for the case of the strong Saharan dust outbreak, the fine-mode and coarse-mode-related AOTs were about 0.16 and 0.61 at 532 nm, respectively, during one of the last Sun photometer measurements on 29 May 2008, 17:30 UTC, about 4 h before the lidar observations in Fig. 2 were performed. The values varied by about 10 % as a function of time and were only slightly lower in the next morning according to the AERONET observations. Together with the lidar-derived column backscatter values CB for the non-depolarizing (fine mode) and depolarizing (coarse mode) particle fractions we obtain column lidar ratios of about 64 sr (fine mode) and 52 sr (coarse mode). These values are typical for anthropogenic, aged, moderately absorbing urban haze (Müller et al., 2007), and for desert dust (Tesche et al., 2009a, 2011a; Groß et al., 2011b), respectively.

Desert dust lidar ratios for this dust event in May 2008 are also presented by Wiegner et al. (2011b). Their Raman lidar observations revealed dust lidar ratios of 59 ± 10 sr at

ACPD
12, 13363–13403, 2012

532 nm and dust depolarization ratios of 30–35 % at this wavelength. Our own Raman lidar observations on that evening yield an AOT for the dust layer of 0.65 (from 500–6000 m) and lidar ratios around 55 sr at both 355 and 532 nm. Thus the consistency of the lidar-photometer observations suggest that the basic assumption of the retrieval scheme is justified.

The very low Ångström exponent (for the total aerosol) in Table 3 indicates the strong influence of desert dust on the spectral AOT in this case. A typical fine-mode Ångström exponent of 1.5 for urban haze was derived. As mentioned, in the retrieval of fine-mode and coarse-mode AOT, the coarse-mode Ångström exponent is set to zero (O'Neill et al., 2003), which is in full agreement with our Raman lidar observation of the extinction coefficients at 355 and 532 nm during this evening.

3.2 Saharan dust mixed with biomass-burning smoke

During the SAMUM-2 campaign in January and February 2008, lofted aerosol layers containing desert dust and biomass-burning smoke were frequently advected across the lidar site at Praia, Cape Verde (Groß et al., 2011b; Tesche et al., 2011a; Toledano et al., 2011). The aerosol stratification in Fig. 3 is typical for the winter season over the eastern tropical North Atlantic (Ben-Ami et al., 2009). During the dry season in Central Africa, a belt with strong fire activity extending over several thousands of kilometers from Western to Eastern Africa produces large amounts of fire smoke which is carried towards the Americas by dust-laden air (Ansmann et al., 2009; Ben-Ami et al., 2010; Baars et al., 2011).

The case, shown in Fig. 3, is discussed by Tesche et al. (2011a,b) and Groß et al. (2011a). Three ground-based SAMUM lidars contributed to Fig. 3. Two of them were optimized for near-range (marine boundary layer, MBL) observations and one for far-range measurements up to the tropopause (< 17 km height). By using a scanning polarization lidar (Groß et al., 2011b) it was possible to obtain accurate particle depolarization ratios with high vertical resolution down to very low heights within the MBL.

ACPD
12, 13363–13403, 2012

The profile of the total particle backscatter coefficient in Fig. 3a indicates strong backscattering within the MBL (top at about 600 m height) and moderate backscattering up to 4 km height. The particle depolarization ratio in Fig. 3b shows values around 24 % throughout the MBL caused by a strong contribution of desert dust to particle backscattering. Only 20 % of MBL backscattering was caused by marine particles on this day. If we keep in mind that the lidar ratios of marine particles and mineral dust are 20 sr and 55 sr, respectively, the marine extinction coefficients were about 20 Mm^{-1} and the ones for desert dust particles 200–250 Mm^{-1} (Fig. 3d), and therefore more than an order of magnitude higher than the marine values.

Accurate particle depolarization ratios were obtained up to 3 km height (Fig. 3b). Above that height we assumed a similar depolarization ratio up to the top of the smoke layer. Particle depolarization ratios from 10–20 % indicate a strong influence of smoke on the optical properties. The backscatter coefficients for fine and coarse mode in Fig. 3c corroborate the hypothesis. Above 1000 m height smoke and dust contributed almost equally to particle backscattering. However, the smoke extinction coefficients were slightly higher than the dust-related ones owing to the fact that the smoke lidar ratio was much larger than the dust lidar ratio (Fig. 3d). Lidar ratios of 55 sr (desert dust, coarse mode) and 75 sr (biomass-burning particles, fine mode) were used in the conversion of backscatter into extinction coefficients.

In the retrieval of the mass concentrations we used $\rho_f = 1.35\,g\,cm^{-3}$, and mean values of $v_c/\tau_c = 0.64 \times 10^{-6}$ m and $v_f/\tau_f = 0.24 \times 10^{-6}$ m (computed from the individual values in Fig. 1, case a). The respective fine-mode and coarse-mode-related mass-specific extinction coefficients are $k_{ext,c} = 0.60\,m^2\,g^{-1}$ and $k_{ext,f} = 3.09\,m^2\,g^{-1}$, respectively.

Because we cannot separate marine and smoke contributions to backscattering in the MBL (both aerosol types do not depolarize laser light), we provide particle mass concentration for the fine mode (smoke) only for heights above the MBL in Fig. 3d. A mean of about 10 $\mu g\,m^{-3}$ of smoke mass concentration was observed on that day with maximum values close to 20 $\mu g\,m^{-3}$. Dust mass concentrations ranged from

ACPD
12, 13363–13403, 2012

300–400 $\mu g\,m^{-3}$ in the MBL and from 25–100 $\mu g\,m^{-3}$ in the free troposphere. We observed similar dust-smoke layers almost continuously during the SAMUM-2 campaign from 15 January to 15 February 2008 (Tesche et al., 2011a,b). Smoke-related particle extinction coefficients ranged from 25–100 Mm^{-1} between 1000 and 5000 m height and indicated smoke particle mass concentrations of 10–35 $\mu g\,m^{-3}$. It is interesting to note that Baars et al. (2011) found fine-mode-related extinction values of 10–70 Mm^{-1} in the Amazon rain forest north of Manaus, Brazil, during the wet season (February to May 2008) caused by long-range transport of African smoke. These extinction values indicate mass concentrations of African smoke particles of 5–20 $\mu g\,m^{-3}$ over the Amazon rain forest.

Water-uptake effects and associated uncertainties in the retrieval of the mass concentrations of dry but hygroscopic smoke particles were estimated to be < 25 %. In most cases, SAMUM radiosonde launches at the lidar site indicated relative humdities below 70–80 %. Saharan dust is almost hydrophobic so that water uptake does not play a role here.

The question may arise why the layer with strong dust backscatter over Cape Verde coincides with the marine boundary layer. This results from very different air mass flows with winds from northeast in the boundary layer and from southerly direction within the smoke-containing air above 600 m height.

The lidar-photometer consistency check revealed good agreement. As can be seen in Table 3, the total AOT was about 0.3, with a dust fraction of 0.6 after eliminating a marine contribution of the order of 0.01 on that day (Groß et al., 2011a). The separation of dust and marine particles by means of the depolarization ratio is described by Groß et al. (2011b). AERONET photometer results for 22 January 2008 are only available as level 1.0 products. However, they are in good agreement with the quality-checked level 2.0 results for 23 January 2008 (early morning) and with observations of a second SAMUM photometer on 22 January 2008 (Toledano et al., 2011).

The dust AOT of 0.18 together with the dust-related (coarse-mode) column backscatter in Table 3 yield a dust column lidar ratio of 51.7 sr which is close to values for pure

ACPD
12, 13363–13403, 2012

dust of around 55 sr (Tesche et al., 2009a). Note the large lidar ratio for the fine mode which indicates strongly absorbing smoke particles (Tesche et al., 2011b). Our Raman lidar observations during that evening show smoke-related lidar ratios from 50–100 sr (on average values of 60–70 sr) at 532 nm for the smoke layer. The photometer-derived fine-mode AOT was 0.11 at about 18:30 UTC, while the Raman lidar observations after 20:00 UTC indicate a value of 0.08–0.09 for the fine-mode AOT at 532 nm so that the column lidar ratio for the smoke fraction was probably in the range of 70–80 sr, and thus 25 % lower than the value of 98 sr in Table 3 during the lidar measurement session. Again, the overall consistency of the entire observational data set is very good after this in-depth check so that the retrieval of mass concentrations is reliable.

3.3 Eyjafjallajökull volcanic aerosol plume

The evolution of the aerosol layering over Leipzig on 19 April 2010, 4–5 days after the strong eruptions of the Icelandic Eyjafjallajökull volcano is discussed by Ansmann et al. (2011a). A characteristic scene from the afternoon of that day is shown in Fig. 4. During this time period, a research aircraft (Falcon aircraft of German Aerospace Center) performed height-resolved in situ aerosol observations over Leipzig from 2–6 km height between 14:51–15:28 UTC (Schumann et al., 2011). The boundary layer reached maximum heights of about 1400 m on 19 April 2010. However, the layer with strong backscattering was almost 3 km deep (Fig. 4a). Above the boundary layer the atmosphere was dry with relative humidities of 50–60 % in the layer from 1.5–3 km height and below 25 % higher up (Schumann et al., 2011). The depolarization ratio in Fig. 4b indicates three layers, one with non-light-depolarizing particles (sulfate, urban haze) up to about 1.6 km, and two layers with considerable depolarization from 1.8–2.8 km and from 3.8–5.5 km height. The latter were caused by a mixture of fine- and coarse-mode particles. The backscatter and extinction profiles for fine and coarse mode show this more quantitatively (Fig. 4c, d). Volcanic dust mass concentrations of up to 250 $\mu g\,m^{-3}$ (1.8–2.8 km height) and 40 $\mu g\,m^{-3}$ (3.8–5.5 km) were derived (Fig. 4e). The aircraft observations revealed values of 50–250 $\mu g\,m^{-3}$ and 15–40 $\mu g\,m^{-3}$ in the respective layers

ACPD
12, 13363–13403, 2012

(Schumann et al., 2011). Relatively well-mixed conditions with mass concentrations of 50–80 $\mu g\,m^{-3}$ were found for the fine-mode fraction in the lowermost 2 km of the atmosphere. Aged sulfate aerosol originating from the volcanic SO_2 plumes considerably contributed to the fine-mode particle mass (about 50 %) on that day (Ansmann et al., 2011a).

The fine- and coarse-mode-related mass-specific extinction coefficients are $k_{ext,c} = 0.64\,m^2\,g^{-1}$ and $k_{ext,f} = 3.47\,m^2\,g^{-1}$ in this case, with mean values of $v_c/\tau_c = 0.60 \times 10^{-6}$ m and $v_f/\tau_f = 0.18 \times 10^{-6}$ m according to Fig. 1 (case c). Lidar ratios of 55 sr (volcanic dust) and 45 sr (sulfate particles, see discussion below) were used in the conversion of the backscatter into particle extinction coefficients shown in Fig. 4d.

The total and fine-mode AOT were unusually high with values of 0.65 and 0.51 at 532 nm, respectively (see Table 3). Together with the CB values we obtain column lidar ratios of about 45 sr (fine mode) and almost 55 sr for the volcanic dust. The fine-mode lidar ratio is typical for non-absorbing accumulation mode particles (Müller et al., 2007). The coarse-mode lidar ratio of 55 sr is characteristic for volcanic dust (Ansmann et al., 2010; Groß et al., 2012).

3.4 Grimsvötn volcanic aerosol

According to reports of the Icelandic Meteorological Office (IMO) the eruptions of the ice-capped Eyjafjallajökull volcano in April 2010 were more explosive than the eruptions of the Grimsvötn volcano in May 2011 (http://en.vedur.is/earthquakes-and-volcanism/articles/nr/2220 and 2221). The latter also started as subglacial eruptions which, however, quickly broke the ice cover. Compared to the Eyjafjalljökull case, the Grimsvötn volcanic eruptions resulted in the release of coarser particulate matter according to the IMO report.

First volcanic plumes reached Central Europe on 24 May 2011, about 2.5 days after the eruptions in the late afternoon of 21 May 2011. Tesche et al. (2012) provides information on the air mass transport towards Central and Northern Europe on

ACPD
12, 13363–13403, 2012

25 May 2011. A consistent air flow from the North Atlantic (Iceland area), across the UK towards Germany prevailed in the lowermost 2 km of the atmosphere on 25 and 26 May 2011 (until noon). Figure 5 presents lidar observations during the passage of the densest volcanic dust plumes. Traces of the volcanic emissions crossed Leipzig up to a height of 4 km on 25 May 2011, 10:00–12:00 UTC. Above 4 km height further aerosol layers were detected. These layers were advected from southwesterly directions according to the transport simulations. They probably originated from North Africa and/or North America (mixture of desert dust and aged urban haze). Such lofted aerosols are a common feature during the summer half year (Mattis et al., 2008). The AOT of the non-volcanic aerosols above 4 km height was estimated to be less than 0.008 and is thus ignored in the following discussion of lidar-photometer observations. The increasing particle depolarization ratio for heights above 6 km in Fig. 5b may not be trustworthy. The uncertainty in the particle depolarization ratio steadily increases when the particle backscatter coefficient approaches zero.

In agreement with the IMO report, the microphysical and optical properties of the Grimsvötn volcanic aerosol were found to be very different from the Eyjafjallajökull volcanic particle characteristics. Figure 1 indicates larger volcanic dust particles in May 2011. The mean value of v_c/τ_c of 0.90×10^{-6} m for the Grimsvötn volcanic dust is 50 % higher than the respective Eyjafjalljökull value of 0.60×10^{-6} m. The coarse-mode-related mass-specific extinction coefficients $k_{ext,c}$ are $0.43\,m^2\,g^{-1}$ for the Grimsvötn aerosol and $0.64\,m^2\,g^{-1}$ for the Eyjafjallajökull particles. The extinction coefficients in Fig. 5d are computed with lidar ratiosof 55 sr for volcanic dust and 40 sr for the fine-mode particles (according to the discussion below).

In contrast to the Eyjafjallajökull volcanic dust plumes (mostly advected in the free troposphere), the Grimsvötn aerosol was found in the lowermost 2 km of the troposphere over Leipzig. On 25 May 2011, the volcanic dust was well-mixed throughout the boundary layer around local noon (see Fig. 5). Cumulus clouds developed from time to time during the measurement as detected with lidar. Therefore, we must assume high relative humidities of > 80 to 90 % in the upper boundary layer, even during cloud-free

ACPD
12, 13363–13403, 2012

periods. At ground the relative humidity ranged from 35–45 % according to the meteorological station of the institute. The high relative humidity in the upper boundary layer must be kept in consideration when discussing the mass concentrations. The profiles in Fig. 5 are computed from signal profiles after cloud–screening. The total backscatter coefficient in Fig. 5a indicates the increasing influence of water uptake by fine-mode as well as by the volcanic dust particles (Lathem et al., 2011). The drop in the depolarization ratio in the upper boundary layer (1400–2000 m) is consistent with a change in the shape properties of the volcanic dust particles. A part of the coarse particles became obviously spherical.

Unfortunately the depolarization values in Fig. 5b are not very trustworthy at heights below 1200 m because the respective measurement channels were not optimized on that day. The signal channel for cross-polarized light showed saturation effects in the near range (< 1200 m height) during this event with unexpectedly strong depolarization return signals. As a consequence we put large uncertainty bars to the boundary layer profile of the particle depolarization ratio below 1200 m. Because there was no layer with pure volcanic dust for the determination of a Grimsvötn volcanic dust depolarization ratio we assume that the volcanic dust depolarization ratio for the Eyjafjallajökull event also holds for the Grimsvötn case. Clearly, more depolarization observations of volcanic dust are needed to allow for a more general and accurate quantification of volcanic dust mass concentrations with polarization lidars.

Because of a potential water-uptake effect, the results in Fig. 5c, d, e are not trustworthy for heights between 1.4 and 2.0 km. Mass concentrations of volcanic dust are reliable for heights <1.2 km and from 2–3 km height. In the lower part of the boundary layer, the volcanic dust mass concentration ranged from 50–90 $\mu g\,m^{-3}$.

Tesche et al. (2012) analyzed in situ surface aerosol observations throughout Scandinavia on 24 and 25 May 2011 and included lidar observations at Stockholm, Sweden, in the study. The main volcanic aerosol plume crossed an area reaching from Northern Germany to Southern and Middle Scandinavia. The time series of the surface observations showed a strong increase in coarse-particle mass concentrations when the first

ACPD
12, 13363–13403, 2012

volcanic dust front crossed the observational site. The peak mass concentrations were close to 160 $\mu g\,m^{-3}$ (Gothenburg, Sweden), 130 $\mu g\,m^{-3}$ (Oslo, Norway, and Stockholm, Sweden) and 100 $\mu g\,m^{-3}$ at Helsinki, Finland (Kerminen et al., 2011). By using the retrieval method presented here, volcanic dust mass concentrations were estimated from the Stockholm lidar observations. The values range from 150–300 $\mu g\,m^{-3}$ in the layer below 2 km height to 150–400 $\mu g\,m^{-3}$ in a lofted layer from 2–4 km height detected in the early morning of 25 May 2011 (Tesche et al., 2012).

The water-uptake effect remains to be discussed in more detail. Lathem et al. (2011) show that volcanic dust particles are hygroscopic. The mean radius of volcanic dust particles was found to increase by 2–10 % when the relative humidity increases from 40 % to 90 %. This means that the effective radius (area-weighted mean radius of the particle size distribution) increases by roughly 5–20 % which in turn leads to an increase in v_c/τ_c by 5–20 % (Gasteiger et al., 2011). On the other hand, water uptake leads to a decrease in particle density from 2.6 to 2.5 $g\,m^{-3}$ (2 % increase of radius) and from 2.6 to 2.1 $g\,m^{-3}$ (10 % increase of radius). Most important however is that an increasing water content changes the shape characteristics of the originally non-spherical particles. A part of the volcanic dust particles obviously became completely spherical during the observation from 10:00–11:50 UTC in Fig. 5 and, as a consequence, the depolarization ratio decreased with height at the top of the well-mixed layer. Large spherical particles show a much higher reflectivity (i.e., backscatter coefficient) than non-spherical particles. According to the extinction-to-backscatter ratio of 55 sr for non-spherical particles and about 20 sr for large spherical particles, the reflectivity is increased by a factor of almost 3.

The large spherical particles are interpreted as fine-mode particles (according to our basic assumption that non-depolarizing particles are fine-mode particles). As a consequence, the column lidar ratio, i.e., the ratio of the fine-mode AOT (from the photometer observations) by the BC caused by spherical particles (assumed to be the fine-mode BC) is rather low (below 25 sr) in Table 3 because of the strong contribution of backscattering of spherical coarse-mode particles to the apparent fine-mode BC. Vice versa, the

ACPD
12, 13363–13403, 2012

CB value for the coarse mode is too low and thus the column lidar ratio too high. A conversion of 10 % of the volcanic non-spherical coarse-mode particles to spherical ones can explain the observed effect and the change of the column lidar ratios from typical values for fine particles of around 40 sr to 22 sr (fine mode) and from typical lidar ratios for volcanic dust of around 50 sr to the observed one of close to 60 sr.

Another interesting feature in Table 3 is the very large fine-mode Ångström exponent of 2.7. This is consistent with the hypothesis that a large number of freshly formed sulfate particles originating from the volcanic SO_2 were present. The corresponding effective radius of 0.11 µm as given in the AERONET data base is very low.

4 Conclusions

We extended the lidar-photometer method introduced for the estimation of volcanic dust mass concentrations to Saharan dust cases. We presented four very different situations of complex aerosol layering with fine and coarse particles. A key parameter in the retrieval of particle mass concentrations is the mass-specific extinction coefficient. Therefore, a review of the recent literature regarding specific extinction coefficients for desert dust and volcanic dust was performed.

We found that the retrieval scheme works well as long as the relative humidity is < 60 % and the water content of the coarse-mode particles is low. In contrast to Saharan dust, volcanic dust particles are hygroscopic. For relative humidities exceeding 80 % the retrieved mass concentrations must be handled with care. Uncertainties are large due to the water-uptake effect and the associated wrong particle classification (fine versus coarse mode), and wrong assumptions in particle density, conversion factors and other input parameters.

The measurements (case studies) showed that Saharan dust loads can be very high over Europe during Saharan dust outbreaks. Mass concentrations of up to 400–500 $\mu g\,m^{-3}$ occurred in the free troposphere (between 1–6 km height) over Central Europe in May 2008. These values are similar to dust loads in the main outflow regime

ACPD
12, 13363–13403, 2012

of Saharan dust over the western tropical Atlantic (Cape Verde). Extended, lofted aerosol layers consisting of mineral dust and biomass-burning particles with smoke mass concentrations of the order of 10–35 $\mu g\,m^{-3}$ were observed over Cape Verde during SAMUM-2 in the winter of 2008.

Volcanic aerosol plumes originating from the Eyjafjallajökull eruptions in April 2010 and the Grimsvötn eruptions observed over Leipzig in May 2011 were contrasted. A striking feature was that the volcanic dust was typically observed above the boundary layer at heights above 2 km in April 2010, while the Grimsvötn aerosol was mainly transported in the well-mixed, moist boundary layer at heights below 2 km.

Based on the four case studies, the retrieval method was shown to be robust and applicable to very different scenarios. The method strongly relies on accurate lidar observations of the particle depolarization ratio. We definitely need more high-quality depolarization observations for volcanic aerosols, such as they are already available for Saharan dust (Freudenthaler et al., 2009; Groß et al., 2011b) or for the Eyjafjallajökull volcanic dust (Ansmann et al., 2011b; Groß et al., 2012). In the case of the Grimsvötn aerosol, depolarization measurements in pure volcanic dust were not possible. Volcanic dust was always mixed with sulfate aerosol.

Acknowledgements. We would like to express our gratitude to the AERONET team for instrument calibration and data analysis. We are grateful to the IfT lidar team for establishing a rich data set of lidar observations.

References

Ansmann, A.: Ground-truth aerosol lidar observations: can the Klett solutions obtained from ground and space be equal for the same aerosol case?, Appl. Optics, 45, 3367–3371, 2006. 13374

Ansmann, A. and Müller, D.: Lidar and atmospheric aerosol particles, in: LIDAR – Range-resolved Optical Remote Sensing of the Atmosphere, edited by: Weitkamp, C., Springer, New York, 105–141, 2005. 13365, 13395

ACPD

12, 13363–13403, 2012

Ansmann, A., Althausen, D., Wandinger, U., Franke, K., Müller, D., Wagner, F., and Heintzenberg, J.: Vertical profiling of the Indian aerosol plume with six-wavelength lidar during INDOEX: a first case study, Geophys. Res. Lett., 27, 7, doi:10.1029/1999GL010902, 2000. 13368

Ansmann, A., Bösenberg, J., Chaikovsky, A., Comerón, A., Eckhardt, S., Eixmann, R., Freudenthaler, V., Ginoux, P., Komguem, L., Linné, H., López Márquez, M. A., Matthias, V., Mattis, I., Mitev, V., Müller, D., Music, S., Nickovic, S., Pelon, J., Sauvage, L., Sobolewsky, P., Srivastava, M. K., Stohl, A., Torres, O., Vaughan, G., Wandinger, U., and Wiegner, M.: Long-range transport of Saharan dust to Northern Europe: the 11–16 October 2001 outbreak observed with EARLINET, J. Geophys. Res., 108, 4783, doi:10.1029/2003JD003757, 2003. 13366, 13370

Ansmann, A., Baars, H., Tesche, M., Müller, D., Althausen, D., Engelmann, R., Pauliquevis, T., and Artaxo, P.: Dust and smoke transport from Africa to South America: lidar profiling over Cape Verde and the Amazon rainforest, Geophys. Res. Lett., 36, L11802, doi:10.1029/2009GL037923, 2009. 13375

Ansmann, A., Tesche, M., Groß, S., Freudenthaler, V., Seifert, P., Hiebsch, A., Schmidt, J., Wandinger, U., Mattis, I., Müller, D., and Wiegner, M.: The 16 April 2010 major volcanic ash plume over Central Europe: EARLINET lidar and AERONET photometer observations at Leipzig and Munich, Germany, Geophys. Res. Lett., 37, L13810, doi:10.1029/2010GL043809, 2010. 13368, 13379, 13396

Ansmann, A., Petzold, A., Kandler, K., Tegen, I., Wendisch, M., Müller, D., Weinzierl, B., Müller, T., and Heintzenberg, J.: Saharan mineral dust experiments SAMUM-1 and SAMUM-2: what have we learned?, Tellus B, 63, 403–429, doi:10.1111/j.1600-0889.2011.00555.x, 2011a. 13364, 13366, 13378, 13379

Ansmann, A., Tesche, M., Seifert, P., Groß, S., Freudenthaler, V., Apituley, A., Wilson, K. M., Serikov, I., Linné, H., Heinold, B., Hiebsch, A., Schnell, F., Schmidt, J., Mattis, I., Wandinger, U., and Wiegner, M.: Ash and fine-mode particle mass profiles from EARLINET-AERONET observations over Central Europe after the eruptions of the Eyjafjallajökull volcano in 2010, J. Geophys. Res., 116, D00U02, doi:10.1029/2010JD015567, 2011b. 13366, 13367, 13369, 13370, 13371, 13384, 13395, 13396, 13397, 13402

Baars, H., Ansmann, A., Althausen, D., Engelmann, R., Artaxo, P., Pauliquevis, T., and Souza, R.: Further evidence for significant smoke transport from Africa to Amazonia, Geophys. Res. Lett., 38, L20802, doi:10.1029/2011GL049200, 2011. 13375, 13377

ACPD
12, 13363–13403, 2012

Barnaba, F. and Gobbi, G. P.: Aerosol seasonal variability over the Mediterranean region and relative impact of maritime, continental and Saharan dust particles over the basin from MODIS data in the year 2001, Atmos. Chem. Phys., 4, 2367–2391, doi:10.5194/acp-4-2367-2004, 2004. 13365, 13369, 13371, 13396, 13397

Ben-Ami, Y., Koren, I., and Altaratz, O.: Patterns of North African dust transport over the Atlantic: winter vs. summer, based on CALIPSO first year data, Atmos. Chem. Phys., 9, 7867–7875, doi:10.5194/acp-9-7867-2009, 2009. 13375

Ben-Ami, Y., Koren, I., Rudich, Y., Artaxo, P., Martin, S. T., and Andreae, M. O.: Transport of North African dust from the Bodélé depression to the Amazon Basin: a case study, Atmos. Chem. Phys., 10, 7533–7544, doi:10.5194/acp-10-7533-2010, 2010. 13375

Bukowiecki, N., Zieger, P., Weingartner, E., Jurányi, Z., Gysel, M., Neininger, B., Schneider, B., Hueglin, C., Ulrich, A., Wichser, A., Henne, S., Brunner, D., Kaegi, R., Schwikowski, M., Tobler, L., Wienhold, F. G., Engel, I., Buchmann, B., Peter, T., and Baltensperger, U.: Ground-based and airborne in-situ measurements of the Eyjafjallajökull volcanic aerosol plume in Switzerland in spring 2010, Atmos. Chem. Phys., 11, 10011–10030, doi:10.5194/acp-11-10011-2011, 2011. 13369

Chaikovsky, A., Dubovik, O., Goloub, P., Tanré, D., Pappalardo, G., Wandinger, U., Chaikovskaja, L., Denisov, S., Grudo, Y., Lopatsin, A., Karol, Y., Lapyonok, T., Korol, M., Osipenko, F., Savitsky, D., Slesar, A., Apituley, A., Alados–Arboledas, L., Binietoglou, I., Comerón, A., Granados–Muñoz, M. J., Papayanis, A., Perrone, M. R., Pietruczuk, A., De Tomasi, F., Wagner, J., and Wang, X.: Algorithm and software for the retrieval of vertical aerosol properties using combined lidar/radiometer data: dissemination in EARLINET network, Proceedings, 26th International Laser Radar Conference, Porto Heli, Greece, 2012. 13364, 13365

Cozic, J., Verheggen, B., Weingartner, E., Crosier, J., Bower, K. N., Flynn, M., Coe, H., Henning, S., Steinbacher, M., Henne, S., Collaud Coen, M., Petzold, A., and Baltensperger, U.: Chemical composition of free tropospheric aerosol for PM1 and coarse mode at the high alpine site Jungfraujoch, Atmos. Chem. Phys., 8, 407–423, doi:10.5194/acp-8-407-2008, 2008. 13369

Devenish, B. J., Thomson, D. J., Marenco, F., Leadbetter, S. J., Ricketts, H., and Dacre, H. F.: A study of the arrival over the United Kingdom in April 2010 of the Eyjafjallajökull ash cloud using ground-based lidar and numerical simulations, Atmos. Environ., 48, 152–164, 2012. 13396

ACPD
12, 13363–13403, 2012

Dubovik, O. and King, M.: A flexible inversion algorithm for retrieval of aerosol optical properties from sun and sky radiance measurements, J. Geophys. Res., 105, 20673–20696, 2000. 13366

Dubovik, O., Sinyuk, A., Lapyonok, T., Holben, B., Mishchenko, M., Yang, P., Eck, T., Volten, H., Muñoz, O., Veihelmann, B., van der Zande, W. J., Leon, J. F., Sorokin, M., and Slutsker, I.: Application of spheroid models to account for aerosol particle non–sphericity in remote sensing of desert dust, J. Geophys. Res., 111, D11208, doi:10.1029/2005JD006619, 2006. 13366

Eck, T. F., Holben, B. N., Reid, J. S., Dubovik, O., Smirnov, A., O'Neill, N. T., Slutsker, I., and Kinne, S.: Wavelength dependence of the optical depth of biomass burning, urban, and desert dust aerosols, J. Geophys. Res., 104, D24, doi:10.1029/1999JD900923, 1999.

Franke, K., Ansmann, A., Müller, D., Althausen, D., Venkataraman, C., Reddy, M. S., Wagner, F., and Scheele, R.: Optical properties of the Indo-Asian haze layer over the tropical Indian Ocean, J. Geophys. Res., 108, 4059, doi:10.1029/2002JD002473, 2003. 13368

Freudenthaler, V., Esselborn, M., Wiegner, M., Heese, B., Tesche, M., Ansmann, A., Müller, D., Althausen, D., Wirth, M., Fix, A., Ehret, G., Knippertz, P., Toledano, C., Gasteiger, J., Garhammer, M., and Seefeldner, M.: Depolarization ratio profiling at several wavelengths in pure Saharan dust during SAMUM 2006, Tellus B, 61, 165–179. doi:10.1111/j.1600-0889.2008.00396.x, 2009. 13365, 13368, 13384, 13395

Gasteiger, J., Groß, S., Freudenthaler, V., and Wiegner, M.: Volcanic ash from Iceland over Munich: mass concentration retrieved from ground-based remote sensing measurements, Atmos. Chem. Phys., 11, 2209–2223, doi:10.5194/acp-11-2209-2011, 2011. 13364, 13365, 13369, 13371, 13382, 13396

Groß, S., Gasteiger, J., Freudenthaler, V., Wiegner, M., Geiß, A., Schladitz, A., Toledano, C., Kandler, K., Tesche, M., Ansmann, A., and Wiedensohler, A.: Characterization of the planetary boundary layer during SAMUM-2 by means of lidar measurements, Tellus B, 63, 695–705, doi:10.1111/j.1600-0889.2011.00557.x, 2011a. 13365, 13366, 13375, 13377, 13401

Groß, S., Tesche, M., Freudenthaler, V., Toledano, C., Wiegner, M., Ansmann, A., Althausen, D., and Seefeldner, M.: Characterization of Saharan dust, marine aerosols and mixtures of biomass-burning aerosols and dust by means of multi-wavelength depolarization and Raman lidar measurements during SAMUM 2, Tellus B, 63, 706–724, doi:10.1111/j.1600-0889.2011.00556.x, 2011b. 13365, 13366, 13367, 13368, 13374, 13375, 13377, 13384, 13401

ACPD
12, 13363–13403, 2012

Groß, S., Freudenthaler, V., Wiegner, M., Gasteiger, J., Geiß, A., and Schnell, F.: Dual-wavelength linear depolarization ratio of volcanic aerosols: lidar measurements of the Eyjafjallajökull plume over Maisach, Germany, Atmos. Environ., 48, 85–96, 2012. 13365, 13368, 13379, 13384

Hervo, M., Quennehen, B., Kristiansen, N. I., Boulon, J., Stohl, A., Fréville, P., Pichon, J.-M., Picard, D., Labazuy, P., Gouhier, M., Roger, J.-C., Colomb, A., Schwarzenboeck, A., and Sellegri, K.: Physical and optical properties of 2010 Eyjafjallajökull volcanic eruption aerosol: ground-based, Lidar and airborne measurements in France, Atmos. Chem. Phys., 12, 1721–1736, doi:10.5194/acp-12-1721-2012, 2012. 13371, 13396

Hess, M., Koepke, P., and Schult, I.: Optical properties of aerosols and clouds: the software package OPAC, B. Am. Meteorol. Soc, 79, 831–844, 1998. 13369, 13396, 13397

Johnson, B. and Osborne, S. R.: Physical and optical properties of mineral dust aerosol measured by aircraft during the GERBILS campaign, Q. J. Roy. Meteor. Soc., 137, 1117–1130, 2011. 13397

Johnson, B. T. T., Turnbull, K. F., Brown, P. R., Burgess, R., Dorsey, J. R., Baran, A. J., Webster, H. N., Haywood, J. M., Cotton, R., Ulanowski, J., Hesse, E., Woolley, A. M., and Rosenberg, P.: In-situ observations of volcanic ash clouds from the FAAM aircraft during the eruption of Eyjafjallajökull in 2010, J. Geophys. Res., 117, D00U24, doi:10.1029/2011JD016760, 2012. 13371, 13396

Kandler, K., Schütz, L., Deutscher, C., Ebert, M., Hofmann, H., Jäckel, S., Jaenicke, R., Knippertz, P., Lieke, K., Massling, A., Petzold, A., Schladitz, A., Weinzierl, B., Wiedensohler, A., Zorn, S., and Weinbruch, S.: Size distribution, mass concentration, chemical and mineralogical composition and derived optical parameters of the boundary layer aerosol at Tinfou, Morocco, during SAMUM 2006, Tellus B, 61, 32–50, doi:10.1111/j.1600-0889.2008.00385.x, 2009. 13370

Kandler, K., Schütz, L., Jäckel, S., Lieke, K., Emmel, C., Müller–Ebert, D., Ebert, M., Scheuvens, D., Schladitz, A., Segvic, B., Wiedensohler, A., and Weinbruch, S.: Ground-based off-line aerosol measurements at Praia, Cape Verde, during the Saharan Mineral Dust Experiment: microphysical properties and mineralogy, Tellus B, 63, 459–474. doi:10.1111/j.1600-0889.2011.00546.x, 2011. 13370

Kerminen, V.-M., Niemi, J. V., Timonen, H., Aurela, M., Frey, A., Carbone, S., Saarikoski, S., Teinilä, K., Hakkarainen, J., Tamminen, J., Vira, J., Prank, M., Sofiev, M., and Hillamo, R.: Characterization of a volcanic ash episode in Southern Finland caused by the Grimsvötn

ACPD
12, 13363–13403, 2012

eruption in Iceland in May 2011, Atmos. Chem. Phys., 11, 12227–12239, doi:10.5194/acp-11-12227-2011, 2011. 13367, 13382

Lathem, T. L., Kumar, P., Nenes, A., Dufek, J., Sokolik, I. N., Trail, M., and Russell, A.: Hygroscopic properties of volcanic ash, Geophys. Res. Lett., 38, L11802, doi:10.1029/2011GL047298, 2011. 13381, 13382

Liu, D., Wang, Z., Liu, Z., Winker, D., and Trepte, C.: A height resolved global view of dust aerosols from the first year CALIPSO lidar measurements, J. Geophys. Res., 113, D16214, doi:10.1029/2007JD009776, 2008. 13365

Marenco, F. and Hogan, R. J.: Determining the contribution of volcanic ash and boundary layer aerosol in backscatter lidar returns: a three-component atmosphere approach, J. Geophys. Res., 116, D00U06, doi:10.1029/2010JD015415, 2011. 13364

Marenco, F., Johnson, B., Turnbull, K., Newman, S., Haywood, J., Webster, H., and Ricketts, H.: Airborne lidar observations of the 2010 Eyjafjallajökull volcanic ash plume, J. Geophys. Res., 116, D00U05, doi:10.1029/2011JD016396, 2011. 13396

Mattis, I., Ansmann, A., Müller, D., Wandinger, U., and Althausen, D.: Dual-wavelength Raman lidar observations of the extinction-to-backscatter ratio of Saharan dust, Geophys. Res. Lett., 29, 1306, doi:10.1029/2002GL014721, 2002. 13365

Mattis, I., Müller, D., Ansmann, A., Wandinger, U., Preißler, J., Seifert, P., and Tesche, M.: Ten years of multiwavelength Raman lidar observations of free-tropopsheric aerosol layers over Central Europe: geometrical properties and annual cycle, J. Geophys. Res., 113, D20202, doi:10.1029/2007JD009636, 2008. 13380

Mattis, I., Seifert, P., Müller, D., Tesche, M., Hiebsch, A., Kanitz, T., Schmidt, J., Finger, F., Wandinger, U., and Ansmann, A.: Volcanic aerosol layers observed with multiwavelength Raman lidar over Central Europe in 2008–2009, J. Geophys. Res., 115, D00L04, doi:10.1029/2009JD013472, 2010. 13365

Miffre, A., David, G., Thomas, B., and Rairoux, P.: Atmospheric non-spherical particles optical properties from UV-polarization lidar and scattering matrix, Geophys. Res. Lett., 38, L16804, doi:10.1029/2011GL048310, 2011. 13364

Miffre, A., David, G., Thomas, B., Rairoux, P., Fjaeraa, A. M., Kristiansen, N. I., and Stohl, A.: Volcanic aerosol optical properties and phase partitioning behavior after long-range advection characterized by UV-Lidar measurements, Atmos. Environ, 48, 76–84, 2012. 13365, 13396

ACPD
12, 13363–13403, 2012

Mona, L., Amodeo, A., D'Amico, G., Giunta, A., Madonna, F., and Pappalardo, G.: Multi-wavelength Raman lidar observations of the Eyjafjallajökull volcanic cloud over Potenza, southern Italy, Atmos. Chem. Phys., 12, 2229–2244, doi:10.5194/acp-12-2229-2012, 2012. 13365

Müller, D., Mattis, I., Wandinger, U., Ansmann, A., Althausen, D., Dubovik, O., Eckhardt, S., and Stohl, A.: Saharan dust over a Central European EARLINET-AERONET site: combined observations with Raman lidar and Sun photometer, J. Geophys. Res., 108, 4345, doi:10.1029/2002JD002918, 2003. 13366, 13370

Müller, D., Ansmann, A., Mattis, I., Tesche, M., Wandinger, U., Althausen, D., and Pisani, G.: Aerosol-type-dependent lidar ratios observed with Raman lidar, J. Geophys. Res., 112, D16202, doi:10.1029/2006JD008292, 2007. 13365, 13368, 13374, 13379

Murayama, T., Okamoto, H., Kaneyasu, N., Kamataki, H., and Miura, K.: Application of lidar depolarization measurement in the atmospheric boundary layer: effects of dust and sea-salt particles, J. Geophys. Res., 104, 31781–31792, doi:10.1029/1999JD900503, 1999. 13365

Nishizawa, T., Okamoto, H., Sugimoto, N., Matsui, I., Shimizu, A., and Aoki, K.: An algorithm that retrieves aerosol properties from dual-wavelength polarized lidar measurements, J. Geophys. Res., 112, D06212, doi:10.1029/2006JD007435, 2007. 13365

O'Neill, N. T., Eck, T. F., Smirnov, A., Holben, B. N., and Thulasiraman, S.: Spectral discrimination of coarse and fine mode optical depth, J. Geophys. Res., 108, 4559, doi:10.1029/2002JD002975, 2003. 13366, 13374, 13375, 13398

Osborne, S. R., Johnson, B. T., Haywood, J. M., Baran, A. J., Harrison, M. A. J., and McConnell, C. L.: Physical and optical properties of mineral dust aerosol during the Dust and Biomass-burning Experiment, J. Geophys. Res., 113, D00C03, doi:10.1029/2007JD009551, 2008. 13397

Papayannis, A., Amiridis, V., Mona, L., Tsaknakis, G., Balis, D., Bösenberg, J., Chaikovski, A., De Tomasi, F., Grigorov, I., Mattis, I., Mitev, V., Müller, D., Nickovic, S., Pérez, C., Pietruczuk, A., Pisani, G., Ravetta, F., Rizi, V., Sicard, M., Trickl, T., Wiegner, M., Gerding, M., Mamouri, R. E., D'Amico, G., and Pappalardo, G.: Systematic lidar observations of Saharan dust over Europe in the frame of EARLINET (2000–2002), J. Geophys. Res., 113, D10204, doi:10.1029/2007JD009028, 2008. 13366

Papayannis, A., Mamouri, R. E., Amiridis, V., Giannakaki, E., Veselovskii, I., Kokkalis, P., Tsaknakis, G., Balis, D., Kristiansen, N. I., Stohl, A., Korenskiy, M., Allakhverdiev, K., Huseyinoglu, M. F., and Baykara, T.: Optical properties and vertical extension of aged ash lay-

ACPD
12, 13363–13403, 2012

ers over the Eastern Mediterranean as observed by Raman lidars during the Eyjafjallajökull eruption in May 2010, Atmos. Environ., 48, 56–65, 2012. 13365, 13368
Pappalardo, G., Amodeo, A., Mona, L., Pandolfi, M., Pergola, N., and Cuomo, V.: Raman lidar observations of aerosol emitted during the 2002 Etna eruption, Geophys. Res. Lett., 31, L05120, doi:10.1029/2003GL019073, 2004. 13365
Reichardt, J., Dörnbrack, A., Reichardt, S., Yang, P., and McGee, T. J.: Mountain wave PSC dynamics and microphysics from ground-based lidar measurements and meteorological modeling, Atmos. Chem. Phys., 4, 1149–1165, doi:10.5194/acp-4-1149-2004, 2004.
Reid, J. S., Koppmann, R., Eck, T. F., and Eleuterio, D. P.: A review of biomass burning emissions part II: intensive physical properties of biomass burning particles, Atmos. Chem. Phys., 5, 799–825, doi:10.5194/acp-5-799-2005, 2005. 13369
Sakai, T., Nagai, T., Zaizen, Y, and Mano, Y.: Backscattering linear depolarization ratio measurements of mineral, sea-salt, and ammonium sulfate particles simulated in a laboratory chamber, Appl. Optics, 49, 4441–4449, 2010. 13367
Sassen, K.: Polarization in lidar, in: LIDAR – Range-resolved Optical Remote Sensing of the Atmosphere, edited by: Weitkamp, C., Springer, New York, 19–42, 2005. 13365
Sassen, K., Zhu, J., Webley, P., Dean, K., and Cobb, P.: Volcanic ash plume identification using polarization lidar: Augustine eruption, Alaska, Geophys. Res. Lett., 34, L08803, doi:10.1029/2006GL027237, 2007. 13365
Schumann, U., Weinzierl, B., Reitebuch, O., Schlager, H., Minikin, A., Forster, C., Baumann, R., Sailer, T., Graf, K., Mannstein, H., Voigt, C., Rahm, S., Simmet, R., Scheibe, M., Lichtenstern, M., Stock, P., Rüba, H., Schäuble, D., Tafferner, A., Rautenhaus, M., Gerz, T., Ziereis, H., Krautstrunk, M., Mallaun, C., Gayet, J.-F., Lieke, K., Kandler, K., Ebert, M., Weinbruch, S., Stohl, A., Gasteiger, J., Groß, S., Freudenthaler, V., Wiegner, M., Ansmann, A., Tesche, M., Olafsson, H., and Sturm, K.: Airborne observations of the Eyjafjalla volcano ash cloud over Europe during air space closure in April and May 2010, Atmos. Chem. Phys., 11, 2245–2279, doi:10.5194/acp-11-2245-2011, 2011. 13378, 13379
Shimizu, A., Sugimoto, N., Matsui, I., Arao, K., Uno, I., Murayama, T., Kagawa, N., Aoki, K., Uchiyama, A., and Yamazaki, A.: Continuous observations of Asian dust and other aerosols by polarization lidars in China and Japan during ACE-Asia, J. Geophys. Res., 109, D19S17, doi:10.1029/2002JD003253, 2004. 13365
Sicard, M., Guerrero-Rascado, J. L., Navas-Guzmán, F., Preißler, J., Molero, F., Tomás, S., Bravo-Aranda, J. A., Comerón, A., Rocadenbosch, F., Wagner, F., Pujadas, M., and Alados-

ACPD
12, 13363–13403, 2012

Arboledas, L.: Monitoring of the Eyjafjallajökull volcanic aerosol plume over the Iberian Peninsula by means of four EARLINET lidar stations, Atmos. Chem. Phys., 12, 3115–3130, doi:10.5194/acp-12-3115-2012, 2012. 13365, 13366, 13396, 13397

Sugimoto, N. and Lee, C. H.: Characteristics of dust aerosols inferred from lidar depolarization measurements at two wavelength, Appl. Optics, 45, 7468–7474, 2006 13365

Sugimoto, N., Uno, I., Nishikawa, M., Shimizu, A., Matsui, I., Dong, X., Chen, Y., and Quan, H.: Record heavy Asian dust in Beijing in 2002: observations and model analysis of recent events, Geophys. Res. Lett., 30, 1640, doi:10.1029/2002GL016349, 2003. 13365

Tang, I. and Munkelwitz, H.: Water activities, densities, and refractive indices of aqueous sulfates and sodium nitrate droplets of atmospheric importance, J. Geophys. Res., 99, D9, doi:10.1029/94JD01345, 1994. 13369

Tesche, M., Ansmann, A., Müller, D., Althausen, D., Mattis, I., Heese, B., Freudenthaler, V., Wiegner, M., Eseelborn, M., Pisani, G., and Knippertz, P.: Vertical profiling of Saharan dust with Raman lidars and airborne HSRL in Southern Morocco during SAMUM, Tellus B, 61, 144–164, doi:10.1111/j.1600-0889.2008.00390.x, 2009a. 13365, 13368, 13374, 13378

Tesche, M., Ansmann, A., Müller, D., Althausen, D., Engelmann, R., Freudenthaler, V., and Groß, S.: Vertically resolved separation of dust and smoke over Cape Verde using multiwavelength Raman and polarization lidars during Saharan Mineral Dust Experiment 2008, J. Geophys. Res., 114, D13202, doi:10.1029/2009JD011862, 2009b. 13365, 13367, 13371, 13395

Tesche, M., Groß, S., Ansmann, A., Müller, D., Althausen, D., Freudenthaler, V., and Esselborn, M.: Profiling of Saharan dust and biomass-burning smoke with multiwavelength polarization Raman lidar at Cape Verde, Tellus, 63B, 649–676, doi:10.1111/j.1600-0889.2011.00548.x, 2011a. 13365, 13366, 13374, 13375, 13377, 13401

Tesche, M., Müller, D., Groß, S., Ansmann, A., Althausen, D., Freudenthaler, V., Weinzierl, B., Veira, A., and Petzold, A.: Optical and microphysical properties of smoke over Cape Verde inferred from multiwavelength lidar measurements, Tellus B, 63, 677–694. doi:10.1111/j.1600-0889.2011.00549.x, 2011b. 13365, 13366, 13367, 13368, 13375, 13377, 13378, 13401

Tesche, M., Glantz, P., Johansson, C., Norman, M., Hiebsch, A., Ansmann, A., Althausen, D., Engelmann, R., and Seifert, P.: Volcanic ash over Scandinavia originating from the Grimsvötn eruptions in May 2011, J. Geophys. Res., 117, D09201, doi:10.1029/2011JD017090, 2012. 13367, 13379, 13381, 13382

ACPD
12, 13363–13403, 2012

Toledano, C., Wiegner, M., Garhammer, M., Seefeldner, M., Gasteiger, J., Müller, D., and Koepke, P.: Spectral aerosol optical depth characterization of desert dust during SAMUM 2006, Tellus B, 61, 216–228, doi:10.1111/j.1600-0889.2008.00382.x, 2009.

Toldedano, C., Wiegner, M., Groß, S., Freudenthaler, V., Gasteiger, J., Müller, D., Müller, T., Schladitz, A., Weinzierl, B., Torres, B., and O'Neill, N. T.: Optical properties of aerosol mixtures derived from sun-sky radiometry during SAMUM-2, Tellus B, 63, 635–648, doi:10.1111/j.1600-0889.2011.00573.x, 2011. 13366, 13375, 13377

Toldedano, C., Bennouna, Y., Cachorro, V., Ortiz de Galisteo, J. P., Stohl, A., Stebel, K., Kristiansen, N. I., Olmo, F. J., Lyamani, H., Obregón, M. A., Estellés, V., Wagner, F., Baldasano, J. M., González-Castanedo, Y., Clarisse, L., and de Frutos, A. M.: Aerosol properties of the Eyjafjallajökull ash derived from sun photometer and satellite observations over the Iberian Peninsula, Atmos. Environ., 48, 22–32, 2012. 13366

Turnbull, K. F., Johnson, B. T., Marenco, F., Haywood, J., Minikin, A., Weinzierl, B., Schlager, H., Schumann, U., Leadbetter, S. J., and Woolley, A. M.: A case study of observations of volcanic ash from the Eyjafjallajökull eruption, Part 1: In situ airborne observations, J. Geophys. Res., 117, D00U12, doi:10.1029/2011JD016688, 2012. 13396

Veselovskii, I., Dubovik, O., Kolgotin, A., Lapyonok, T., Di Girolamo, P., Summa, D., Whiteman, D. N., Mishchenko, M., and Tanré, D.: Application of randomly oriented spheroids for retrieval of dust particle parameters from multiwavelength lidar measurements, J. Geophys. Res., 115, D21203, doi:10.1029/2010JD014139, 2010. 13365

Veselovskii, I., Tesche, M., Müller D., Kolgotin, A., and Ansmann, A.: Retrieval of desert dust physical properties from multiwavelength lidar observations obtained during the SAMUM campaigns, J. Geophys. Res., submitted, 2012. 13365, 13397

Wagner, J., Wandinger, U., Ansmann, A., Seifert, P., and Chaikovsky, A.: Evaluation of a combined lidar and sunphotometer retrieval algorithm to determine aerosol microphysical properties, Proceedings, 26th International Laser Radar Conference, Porto Heli, Greece, 2012. 13364

Wang, X., Boselli, A., D'Avinoa, L., Pisani, G., Spinelli, N., Amodeo, A., Chaikovsky, A., Wiegner, M., Nickovic, S., Papayannis, A., Perrone, M. R., Rizzi, V., Sauvage, J., and Stohl, A.: Volcanic dust characterization by EARLINET during Etna's eruptions in 2001–2002, Atmos. Environ., 42, 893–905, 2008. 13365

Weinzierl, B., Petzold, A., Esselborn, M., Wirth, M., Rasp, K., Kandler, K., Schütz, L., Koepke, P., and Fiebig, M.: Airborne measurements of dust layer properties, particle size

ACPD
12, 13363–13403, 2012

distribution and mixing state of Saharan dust during SAMUM 2006, Tellus B, 61, 96–117, doi:10.1111/j.1600-0889.2008.00392.x, 2009. 13370, 13397

Wiegner, M., Gasteiger, J., Groß, S., Schnell, F., Freudenthaler, V., and Forkel, R.: Characterization of the Eyjafjallajökull ash-plume: potential of lidar remote sensing, Phys. Chem. Earth, 36, doi:10.1016/j.pce.2011.01.006, in press, 2011a. 13365, 13368

Wiegner, M., Groß, S., Freudenthaler, V., Schnell, F., and Gasteiger, J.: The May/June 2008 Saharan dust event over Munich: intensive aerosol parameters from lidar measurements, J. Geophys. Res., 116, D23213, doi:10.1029/2011JD016619, 2011b. 13365, 13366, 13368, 13370, 13372, 13374

ACPD

12, 13363–13403, 2012

Table 1. The seven steps of the retrieval to obtain profiles of coarse and fine particle mass concentrations from polarization lidar observations (with support from Sun photometry, step 6). Indices v, t, c, and f denote volume (molecules plus particles), total (fine plus coarse mode), coarse mode, and fine mode, respectively. The methods applied in the different steps are described in the respective reference.

Step	Computed parameter		Reference
1	Volume linear depolarization ratio	δ_v	Freudenthaler et al. (2009)
2	Particle backscatter coefficient	β_t	Ansmann and Müller (2005)
3	Particle linear depolarization ratio	δ_t	Tesche et al. (2009b)
4	Coarse and fine-mode backscatter coefficients	β_c, β_f	Tesche et al. (2009b)
5	Coarse and fine-mode extinction coefficients	σ_c, σ_f	Tesche et al. (2009b); Ansmann et al. (2011b)
6	Coarse and fine-mode volume-to-extinction ratios	v_c/τ_c, v_f/τ_f	Ansmann et al. (2011b)
7	Coarse and fine particle mass concentrations	m_c, m_f	Ansmann et al. (2011b)

ACPD
12, 13363–13403, 2012

Table 2. Overview of recently observed mass-specific extinction coefficients $k_{ext} = \sigma_{ext}/(\rho V)$ for volcanic and desert dust aerosols. In addition the ratio of frequently measured volume concentration to volume extinction coefficient $V/\sigma_{ext} = 1/(k_{ext}\rho)$ is given. A few modelled values (Hess et al., 1998; Barnaba and Gobbi, 2004) for coarse-mode as well as for fine-mode particles are added. Values are mainly taken from the indicated literature (reference). Saharan dust mass-specific extinction coefficients (mean values for the vertical tropospheric column) computed from AERONET Sun photometer observations at Leipzig, Germany, Ouarzazate, Morocco, and Praia, Cape Verde, are included (this study). The mass-specific extinction coefficients hold for a coarse-mode particle density of $\rho_c = 2.6\,g\,cm^{-3}$ (desert and volcanic dust), fine-mode particle density of $\rho_f = 1.6\,g\,cm^{-3}$, and particle extinction coefficients for the 500–550 nm wavelength range. Mean values and/or the range of observed values are given. Hervo et al. (2012) derived mass-specific extinction coefficients for volcanic dust without assumptions of particle mass density.

Reference	k_{ext} [$m^2\,g^{-1}$]	$1/(k_{ext}\rho)$ [$10^{-6}\,m^{-1}$]	Comment
Eyjafjallajökull volcanic dust, Apr–May 2010			
Johnson et al. (2012)	0.40–0.95 0.53	0.96–0.40 0.72	Airborne, in situ, near volcanic source, North Sea >1000 km distance from source, North Sea, UK
Marenco et al. (2011)	0.53–0.80	0.72–0.48	Airborne, in situ, lidar, North Sea, UK
Turnbull et al. (2012)	0.53–0.71	0.72–0.54	Airborne, in situ, North Sea
Hervo et al. (2012)	0.64	0.60	Ground-based, in situ, 1.5 km height, France
Gasteiger et al. (2011)	0.69 (0.43–1.11)	0.56 (0.89–0.35)	Scattering model, lidar, photometer, Germany
Miffre et al. (2012)	0.69 ± 0.10	0.56 ± 0.09	Scattering model, lidar, France
Ansmann et al. (2010)	0.51	0.75	AERONET, remote sensing, first ash front (16 April), very large particles, Central Germany
Devenish et al. (2012)	0.53	0.72	AERONET, remote sensing, first ash front (16 April), very large particles, Southern UK
Ansmann et al. (2011b)	0.64 ± 0.10	0.60 ± 0.10	AERONET, remote sensing, Germany
Sicard et al. (2012)	0.43 ± 0.04	0.90 ± 0.09	AERONET, remote sensing, Spain

ACPD
12, 13363–13403, 2012

Table 2. Continued.

Reference	k_{ext} [$m^2 g^{-1}$]	$1/(k_{ext}\rho)$ [$10^{-6} m^{-1}$]	Comment
Grimsvötn volcanic dust, May 2011			
This study	0.43±0.05	0.90±0.05	AERONET, remote sensing, Germany
Saharan dust			
Hess et al. (1998)	0.64	0.60	OPAC model
Hess et al. (1998)	0.37	1.03	OPAC model, transported dust, free troposphere
Barnaba and Gobbi (2004)	0.30–1.35	1.28–0.28	Modeling study, full range of realistic size distributions
Johnson and Osborne (2011)	0.48 ± 0.10	0.80 ± 0.20	GERBILS, airborne, in situ, western and west of Africa
Osborne et al. (2008)	0.30–0.40	1.29–0.96	DABEX, DODO1, airborne, in situ, western Africa
Weinzierl et al. (2009)	0.45–0.70	0.85–0.55	SAMUM-1, airborne, in situ, South Morocco, > 2 km height
Veselovskii et al. (2012)	0.57 ± 0.04	0.68 ± 0.05	SAMUM-1, multi-λ lidar, South Morocco, > 2 km height
This study	0.50 ± 0.05	0.77 ± 0.07	AERONET, remote sensing, Germany, Oct. 2001, May 2008
This study	0.52 ± 0.03	0.74 ± 0.04	SAMUM-1, AERONET, remote sensing, South Morocco
This study	0.52 ± 0.06	0.74 ± 0.08	SAMUM-2, AERONET, remote sensing, Cape Verde
Continental particles (fine mode)			
Hess et al. (1998)	1.80 (2.40)	0.35 (0.26)	OPAC model, clean continental, rel. humidity 50 % (80 %)
Hess et al. (1998)	2.20 (2.90)	0.28 (0.22)	OPAC model, polluted continental, rel. humidity 50 % (80 %)
Barnaba and Gobbi (2004)	3.00–4.00	0.21–0.16	Modeling study, full range of realistic size distributions
Ansmann et al. (2011b)	3.50 ± 0.02	0.18 ± 0.02	AERONET, remote sensing, Germany
Sicard et al. (2012)	2.40 ± 0.02	0.25 ± 0.01	AERONET, remote sensing, Spain

ACPD
12, 13363–13403, 2012

Table 3. Aerosol optical thickness (AOT), column-integrated backscatter coefficient (CB in sr^{-1}), and column lidar ratio (AOT/CB in sr) for the four case studies shown in Figs. 2–5. All values are given for 532 nm wavelength. Ångström exponents (AE) after O'Neill et al. (2003) for the spectral range around 500 nm are shown in addition.

Case study, observation times, location	Aerosol	AOT	CB	AOT/CB	AE
Saharan dust/urban haze,	total	0.770	0.01414	54.4	0.29
AOT (17:22 UTC), CB (21:47–23:20 UTC), Leipzig, 29 May 2008	fine coarse	0.162 0.608	0.00253 0.01161	64.1 52.4	1.49 0
Saharan dust/smoke/marine,	total	0.301	0.00536	56.2	0.47
AOT (18:32–18:37 UTC), CB (20:05–21:00 UTC), Praia, 22 Jan 2008	smoke coarse dust	0.107 0.194 0.182	0.00109 0.00427 0.00352	98.2 45.4 51.7	1.48 0 0
Volcanic dust/sulfate/urban haze,	total	0.649	0.01369	47.4	1.12
AOT (14:38–15:37 UTC), CB (14:35–15:36 UTC), Leipzig, 19 Apr 2010	fine coarse	0.506 0.143	0.01135 0.00261	44.6 54.8	1.45 0
Volcanic dust/sulfate/urban haze,	total	0.130	0.00376	34.6	1.19
AOT (09:53–11:53 UTC), CB (10:00–11:50 UTC), Leipzig, 25 May 2011	fine coarse	0.055 0.075	0.00248 0.00128	22.2 58.6	2.72 0

ACPD
12, 13363–13403, 2012

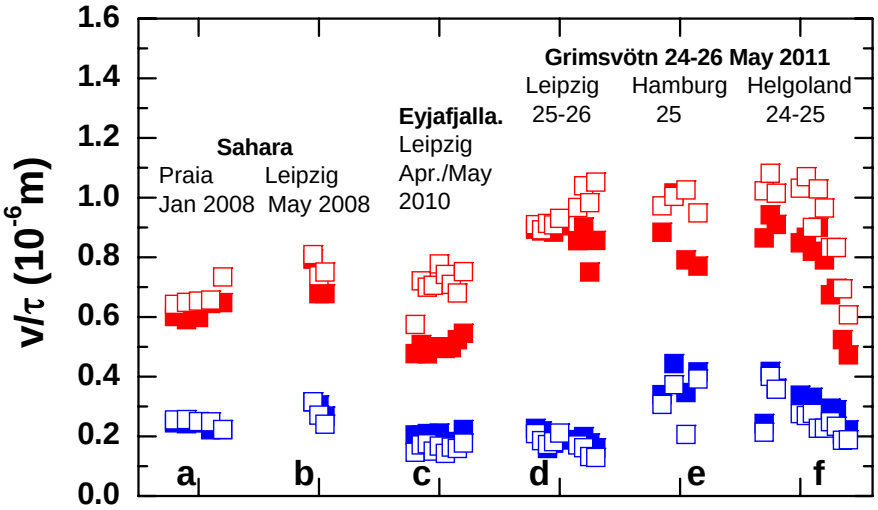

Fig. 1. Ratio v/τ of column volume concentration v to AOT τ at 532 nm for coarse (red) and fine particles (blue). The ratios are derived from AERONET Sun photometer measurements in **(a)** mixed desert-dust/biomass-burning-smoke plumes at Praia, Cape Verde in January 2008, **(b)** during a strong Saharan dust outbreak at Leipzig in May 2008, **(c)** during the Eyjafjallajökull volcanic dust event (Leipzig, April–May 2010), and **(d–f)** the Grimsvötn volcanic dust episode (Helgoland, Hamburg, Leipzig, May 2011). Fine-mode and coarse-mode τ values were calculated by using the Dubovik approach (open symbols) and the O'Neill method (closed symbols). See text for more details.

ACPD
12, 13363–13403, 2012

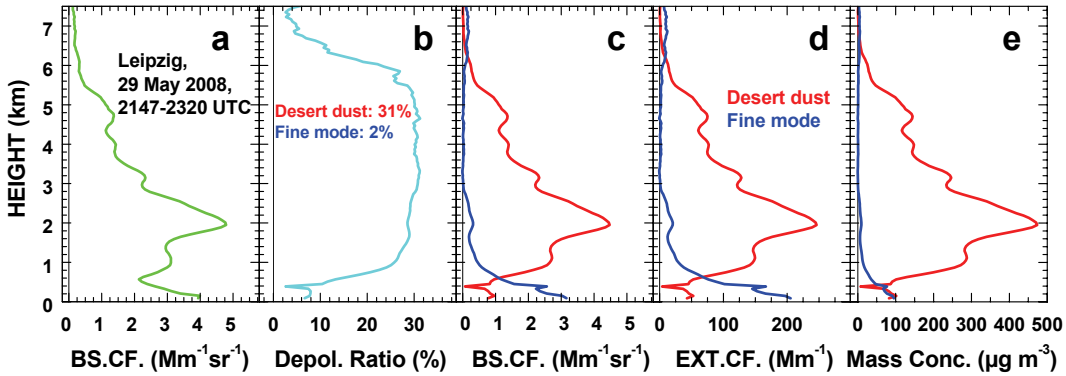

Fig. 2. (a) 532 nm particle backscatter coefficient, **(b)** 532 nm particle linear depolarization ratio, **(c)** fine-mode (blue) and coarse-mode (red) particle backscatter coefficients, **(d)** fine-mode (blue) and coarse-mode (red) particle extinction coefficients, **(e)** and fine-mode (blue) and coarse-mode (red) particle mass concentrations. The lidar observations were taken at Leipzig in May 2008.

ACPD
12, 13363–13403, 2012

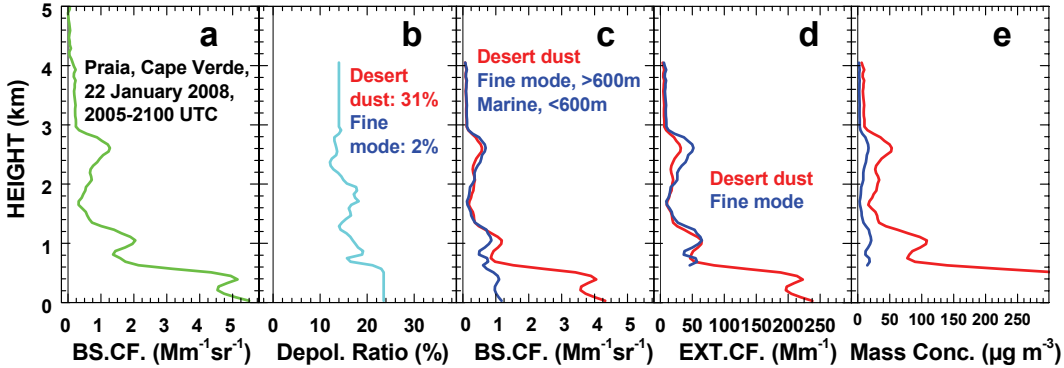

Fig. 3. Same as Fig. 2 except for a SAMUM-2 lidar observation at Praia, Cape Verde, in January 2008. Composite profiles of backscatter and extinction coefficients and depolarization ratio are shown, derived from measurements with three lidars (Groß et al., 2011a,b; Tesche et al., 2011a,b). In **(c)**, >600 m and <600 m refer to the height range above and within the MBL with layer top height of 600 m, respectively.

ACPD
12, 13363–13403, 2012

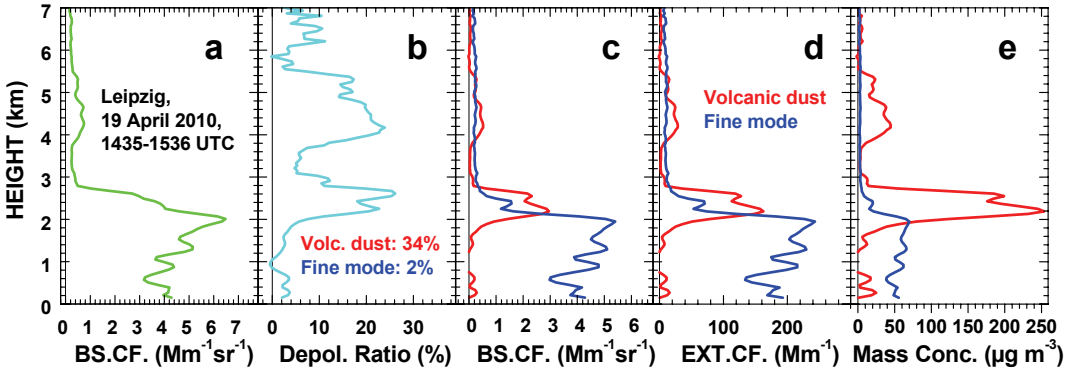

Fig. 4. Same as Fig. 2 except for Eyjafjallajökull volcanic aerosol observed at Leipzig in April 2010 (Ansmann et al., 2011b).

ACPD
12, 13363–13403, 2012

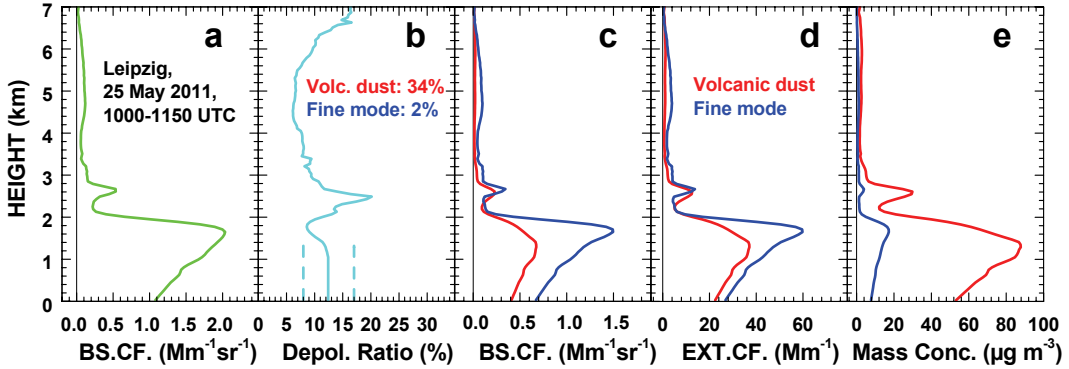

Fig. 5. Same as Fig. 2 except for Grimsvötn volcanic aerosol observed at Leipzig in May 2011. Dashed lines in **(b)** indicate the uncertainty range of derived values.

ACPD
12, 13363–13403, 2012